Cement & Concrete Composites 34 (2012) 384–391

Contents lists available at SciVerse ScienceDirect

Cement & Concrete Composites

journal homepage: www.elsevier.com/locate/cemconcomp

Comparative study of accelerated decalcification process among C_3S, grey and white cement pastes

F. Puertas [a,b,*], S. Goñi [a,b], M.S. Hernández [a], C. Varga [a], A. Guerrero [a,b]

[a] Eduardo Torroja Institute for Construction Sciences (IETcc-CSIC), C/ Serrano Galvache 4, 28033 Madrid, Spain
[b] Nanostructured and Eco-efficient Materials for Construction Unit, Associated Unit LABEIN-Tecnalia/CSIC, IETcc, Spain

ARTICLE INFO

Article history:
Received 9 March 2011
Received in revised form 17 October 2011
Accepted 5 November 2011
Available online 12 November 2011

Keywords:
Ca-leaching
Cement pastes
Microstructure
Decalcification
Nanoporosity

ABSTRACT

This study compared the resistance of Triclinic-C_3S, grey (OPC) and white (WOPC) Portland cement paste to decalcification induced by accelerated leaching in concentrated ammonium nitrate solutions. Paste microstructure was studied with scanning and backscattering electron microscopy (SEM and BSEM) and nitrogen BET surface area techniques. Ca^{2+} leached content was quantified by ICP, XRD and FTIR techniques were used to study phase mineralogy. The conclusions drawn from the findings were that calcium leaching-induced decay in the cementitious materials studied (C_3S, OPC and WOPC), accelerated by immersion in ammonium nitrate, affected the main calcium phases in the samples (CH, C–S–H gel and ettringite), i.e., both the anhydrous and the hydrated phases. The present study showed that the Ca/Si ratio of C–S–H gels declines on a gradient from the sample core outward. Specimen surface area and nanoporosity rose in cementitious materials after Ca leaching-induced decay and subsequently declined as a result of the collapse of the structure of the hydrated cement, and in particular of the C–S–H gel. C_3S paste was impacted more quickly and intensely by leaching than the WOPC and OPC pastes. Further to the findings of this study, the leaching resistance of these three materials, in descending order, is: OPC > WOPC > C_3S.

1. Introduction

Concrete made with Portland cement is a porous material vulnerable to physical and chemical attack by aggressive agents [1–4]. The result of such attacks (often induced simultaneously by several agents) is concrete decay characterised by a loss of mass, consistency and strength. A variety of aggressive agents can cause this damage, some of which are merely physical, such as abrasion/erosion or extreme temperatures [5], while others involve chemical action such as internal (DEF) or external sulfate ion attack [6,7], alkali-aggregate reactions [8] or reinforcing steel corrosion. Water plays a role in the vast majority of these developments, particularly where chemical action is involved, for it is an ideal medium for carrying aggressive agents inward into the concrete. Water and its corrosive solutes are regarded to be the primary causes of deterioration in cement paste components [9]. Cement paste and cement hydrated component solubility in water has been studied by a number of authors [10–16]. The water solubility of the main hydrated phases in cement, in descending order, is: $S_{Ca(OH)_2} > S_{AFm} > S_{Friedel's\ salt} > S_{AFt} > S_{C-S-H}$ [6,14].

Aggressive agents such as deionised water, aqueous acid solutions and CO_2 induce the dissolution and decalcification of the main hydration components in both Portland [17–19] and alkali-activated slag [20,21] cements. Due to its greater solubility, portlandite is the first phase to dissolve, forming readily leachable soluble salts or calcium carbonates that precipitate in the concrete pores. If the aggressive agent persists, ettringite and the C–S–H gel decalcify, forming soluble calcium salts and aluminium hydroxide when ettringite is impacted, and low Ca/Si ratio calcium silicate hydrates or even silica gels when the C–S–H gel is attacked [22,23].

Given the low Ca^{2+} diffusion coefficient for concrete, mortar and cement paste, decalcification is a very slow process that must be accelerated in laboratory trials simulating material decay to accurately model the processes involved. A number of acceleration methods have been proposed. Saito et al. [9] used ionised water and electrical gradients that accelerated the cement paste dissolution rate 60-fold. The most effective accelerated decalcification method is leaching in a concentrated ammonium nitrate solution [24–26,33–36]. With this method C–S–H gel decalcification peaks in a matter of days, whereas under normal conditions the process is measured in years. Moreover, the ammonium nitrate medium induces C–S–H gel decalcification without altering the Si content in the gel structure [33].

Thomas et al. [33] studied the effects of decalcification on the microstructure and surface area of white Portland cement (WOPC)

* Corresponding author. Address: Eduardo Torroja Institute for Construction Sciences (IETcc-CSIC), C/Serrano Galvache 4, 28033 Madrid, Spain. Tel.: +34 913020440; fax: +34 913020700.
E-mail address: puertasf@ietcc.csic.es (F. Puertas).

0958-9465/$ - see front matter © 2011 Elsevier Ltd. All rights reserved.
doi:10.1016/j.cemconcomp.2011.11.002

and tricalcium silicate pastes by leaching in concentrated ammonium nitrate solutions. The microstructure and surface area were measured using both small angle neutron scattering (SANS) and nitrogen gas sorption. The authors reported that the SANS values for the volume fractal C–S–H gel phase increased significantly with leaching, and the total surface area per unit of specimen volume measured by SANS doubled with leaching when Ca/Si declined from 3.0 to close to 1.0. The nitrogen BET surface area of WOPC pastes increased with decalcification as well, although not as sharply.

Chen et al. [19] studied decalcification shrinkage in tricalcium silicate paste, WOPC paste, and WOPC paste blended with 30 % silica fume (WOPC/30%SF), likewise by leaching in concentrated solutions of ammonium nitrate. They found that all the pastes shrank significantly and irreversibly as a result of decalcification, particularly when the Ca/Si ratio of the C–S–H gel dropped below 1.2. This composition concurs with the onset of structural changes in C–S–H, such as more intense silicate polymerisation and local densification into a sheet-like morphology. The observed shrinkage, which the authors called decalcification shrinkage, was proposed to be initially due to these structural changes in C–S–H at Ca/Si 1.2 and ultimately to the decomposition of C–S–H into silica gel. Further to this reasoning, the blended cement paste exhibited greater decalcification shrinkage than the pure cement pastes due to its lower initial Ca/Si ratio in the C–S–H gel.

Constantinides and Ulm [34] used nanoindentation tests to study two types of C–S–H in untreated cement paste and paste leached in a concentrated ammonium nitrate solution. These authors explored the differential role played by the two phases on the elastic properties of cement-based materials. They found that: (i) mechanical properties were less affected by calcium leaching in high density than low density C–S–H, and (ii) the volume fractions occupied by the two phases in the C–S–H matrix were unaffected by calcium leaching.

Gaitero et al. [35] studied the decline in the calcium leaching rate in cement paste with the addition of silica nanoparticles. They found that nanosilica increased the strength of the cement paste by around 30% in cured samples and by over 100% in leached specimens. Silica nanoparticles increased the average length of the silicate chains in the C–S–H gel. Degradation, in terms of porosity and the amount of calcium lost, was also observed to drop significantly.

A number of authors have studied and modelled Ca leaching in cements. Berner [10] and Faucon et al. [27] developed models based on cement paste dissolution to evaluate the long-term composition of the liquid and solid phases. Carde et al. [24] and Adenot [28] deemed that the transport mechanism for leached materials was diffusion, while Garrabrants et al. [18] proposed a dual model involving diffusion and solid phase dissolution/precipitation. Calcium leaching is generally regarded to involve a coupled diffusion–dissolution process with clearly defined dissolution fronts that spread across the structure [26].

Whereas the decalcification process of C_3S or white cements has been studied, the literature lacks a comparative study among cement pastes with different mineralogical composition and Ca-contents. The main contribution of the present paper is to compare the behaviour of Triclinic-C_3S, grey (OPC) and white (WOPC) Portland cement paste due to decalcification induced by accelerated leaching in concentrated ammonium nitrate solutions, using a combination of macro-, micro- and nano-techniques for characterisation of the samples before and after exposure to the aggressive medium.

2. Experimental

2.1. Materials

The materials used were: synthesised Triclinic (T1)-C_3S [29] and grey (CEM I 42.4R, abbreviated here as OPC) and white (BL 52.5 R, abbreviated here as WOPC) cements. The chemical composition and particle size distribution for these cements are given in Table 1. The quantitative XRD findings for OPC and WOPC are given in Table 2.

2.2. Paste preparation

The specimens were prepared by mixing the cementitious material with distilled and decarbonated water (water/solid ratio of 0.4) and pouring the pastes into $1 \times 1 \times 6$-cm steel moulds. The prisms were stored at room temperature and ~100% RH inside a container with distilled and decarbonated water for 24 h. Upon removal from the moulds, they were wrapped in aluminium foil and returned to the container for curing under the same conditions for a further 27 days. All these operations were conducted in an inert N_2 atmosphere inside an "Atmosbag".

2.3. Leaching procedure

The T1-C_3S, OPC and WOPC samples were exposed to aggressive calcium leaching as described by Heukamp et al. [26]. This method consists in mantainig the paste cement samples (after 28 of curing) immersed in the 6-M ammonium nitrate solution to accelerated leaching. The main experimental conditions of this method are used in the present research and are described below.

These specimens were hung, fully immersed, in the aggressive solution, 6-M, pH = 5.28 ammonium nitrate, for 9, 21, 42 and 63 days. Since the pH of the aggressive solution had to be kept lower than 9.25, this parameter was measured twice a week. After 30 days, when the pH rose to 9.8 in both cements, the specimens were immersed in a fresh ammonium nitrate solution, which is the "second solution" referred to in the 42-day data. The C_3S specimens had to be placed in a fresh solution after 7 days.

The solid specimens were washed after removal in decarbonated water for around 10 min to eliminate any possible trace of ammonium nitrate on the surface and stored in a vacuum chamber for 2 h to eliminate the strong odour. Part of each solid sample was then ground and mixed with a small volume of acetone to detain further sample hydration, and rinsed with ethanol to facilitate drying. This powdery sample was used for the XRD and FTIR characterisation studies, while the non-ground portion of the specimens was stained with phenolphthalein (as per Spanish standard UNE 112-011-94) for the stereoscopic optical microscopy, BET-N_2 adsorption and BSE/EDX trials.

2.4. Instrumental techniques

The Ca^{2+} content was determined in 20-ml aliquots of the solution at each age on a LEEMAN INC. Direct Reading Echelle inductively coupled plasma atomic emission spectrometer (ICP-OES). The particle size distribution of the C_3S and the cements was measured by laser diffraction (Sympatec Helos 12 KA diffractometer fitted with an He/Ne, 5-mW light source), using isopropyl alcohol as a dispersant and ultrasound to disaggregate particles prior to measurement. Surface area measurements were made on a Micromeritics Instrument Corp. ASAP 2010 analyser using N_2-77 K gas. The surface areas were calculated from the sorption isotherm data with the BET method [36] in a relative pressure range of 0.003–0.3. Pore volume and pore size distributions were found as per the Barret-Joyner-Halenda (BJH) method [37] with data from the adsorption arm of the isotherm. The Harkins and Jura equation [38] was used to calculate the thickness (t) of the layer adsorbed onto the pore walls for each P/Po ratio (see equation [1]):

$$t = [13.99/0.034 - \log_{10}(P/Po)]^{1/2} \quad (1)$$

Table 1
Chemical composition and particle size distribution of OPC and WOPC (wt%).

Cement	SiO_2	Al_2O_3	Fe_2O_3	CaO	MgO	SO_3	Na_2O	K_2O	TiO_2	SrO	P_2O_5	MnO	BaO	CO_2	Cl	L.I.
OPC	18	4.2	2.2	64	3.2	4.5	0.52	1.0	0.22	0.10	0.09	0.04	003	1.8	0.06	1.8
WOPC	19	3.3	0.26	68	1.8	3.6	1.3	0.41	0.03	0.05	0.10	1.7	0.13	1.8	–	1.8

	<10% (μm)	<50% (μm)	<90% (μm)
C_3S	3.27	9.8	31.2
OPC	1.32	8.8	28.0
WOPC	2.14	15.5	37.4

L.I. Loss on ignition.

Table 2
Quantitative XRD characterisation of OPC and WOPC cements.

Phase (wt%)	C_3S	C_2S	C_3A	C_4AF	MgO	Gypsum	Anhydrite
Grey cement	65.7	10.5	8.4	8.4	2.7	1.9	2.3
White cement	87.1	6.0	1.1	–	–	4.1	1.7

Polished surfaces of the samples were examined with backscattered electron imaging (BSEM). The samples were impregnated with epoxy resin, cut, polished and carbon coated. They were studied with a JEOL JSM 5400 scanning electron microscope fitted with a solid-state backscattered detector and a LINK-ISIS energy-dispersive X-ray (EDX) microanalyser. A Nikon Japan (Tv lens c-0.45) stereoscopic optical microscope (SOM) with a KAPPA recording camera was used to observe the advancing front of the aggressive medium.

X-ray diffraction patterns were recorded on a BRUKER D8 ADANCE diffractometer operating at a wavelength of 1.5404 (λCu kα) and at 2θ intervals of 5–60°. A NICOLET 6700 FTIR spectrometer was used for the FTIR analyses. The scan range was 4000–400 cm^{-1}.

3. Results and discussion

3.1. Calcium leaching analysis

The amount of total calcium leached from each specimen was deduced from the calcium analyses conducted on the aggressive solution. The percentage of Ca leached into the medium over the total Ca in the starting material is shown in Fig. 1. The decalcification rate was higher in the C_3S than in either of the cements. Over 90% of the total Ca had leached out of the C_3S after 9 days. The 21-day results for OPC and WOPC were 82% and 87%, respectively. By the end of the test, nearly 100% of the Ca had leached out of all three materials. Of the two cements, OPC was found to be slightly more resistant to leaching than WOPC, as subsequently confirmed by other analytical techniques. These results show a direct relationship between the Ca-content in the cements and their decalcification.

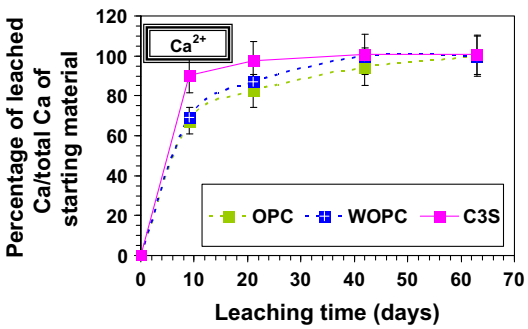

Fig. 1. Ca leaching out of C_3S, OPC and WOPC: % of total Ca in starting material.

3.2. Stereoscopic optical microscopy (phenolphthalein treatment)

The front in the C_3S, OPC and WOPC pastes exposed to the aggressive medium was more readily visible when the materials were treated with phenolphthalein as described in Spanish standard UNE 112-011-94. Fig. 2 compares the 28-day hydrated, phenolphthalein-stained C_3S, OPC and WOPC pastes before exposure to ammonium nitrate and after 9 and 21 days of interaction with the solution.

The decline in the pore solution pH induced by the ammonium nitrate rendered the initially phenolphthalein-stained red–purple specimens colourless. This feature of the indicator was used to track the position of the front.

The front advanced inward evenly across the entire surface of the cross-section. The area in the OPC and WOPC pastes that had not yet interacted with the ammonium nitrate solution after 9 days, i.e., where the pH values were higher than 9.5 (red–purple stain at the core of the specimen), could be approximately measured. The loss of colour in the indicator in the outer-most area denoted greater acidity, with pH values of fewer than 8, due to the decomposition of portlandite and the formation of new compounds deriving from its reaction with the aggressive medium. The 9-day C_3S sample was colourless across the entire surface, an indication that the aggressive solution had penetrated into the inner-most area of the specimen.

3.3. BET-N_2 surface area

The BET-N_2 analyses of the post-leached C_3S, OPC and WOPC pastes revealed that the surface area increased substantially with

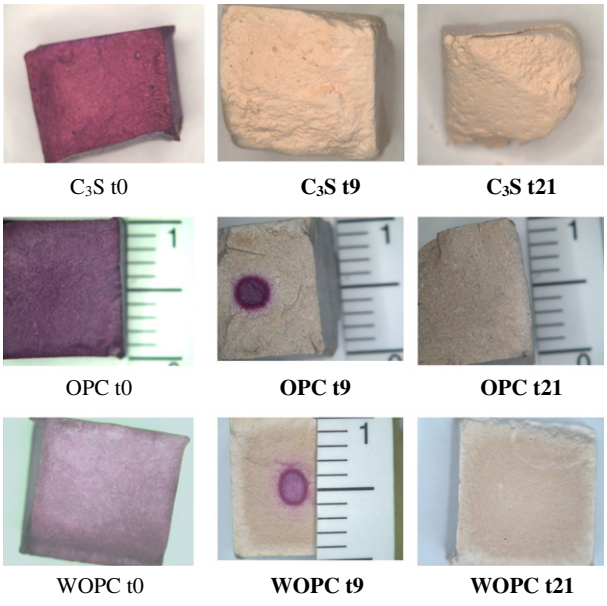

Fig. 2. Stereoscopic optical microscopic images of phenolphthalein-stained C_3S, OPC and WOPC specimen cross-sections: before exposure (t0) and after exposure to the aggressive medium for 9 and 21 days (t9 and t21, respectively).

the progressive decay of the material as a result of the attack. It peaked after 9 days in C_3S and 21 and 42 days in WOPC and OPC, respectively, declining thereafter (see Fig. 3). These results concurred with the findings reported by Thomas et al. [33]. These authors attributed the leaching-induced increase in the BET-N_2 surface area of WOPC and C_3S pastes to the transformation of the high density, low specific area "inner product" C–S–H gel into low density, high specific surface "outer product" C–S–H gel, which forms in the water-filled capillary spaces of the paste. The volume fractal exponent for the C–S–H gel phase decreased with decalcification from 2.3 to 2.0. This datum was an indication that the equiaxed 5-nm C–S–H globule building blocks that form the volume fractal microstructure of normal, unleached cement paste were transformed by decalcification into sheet-like structures of increasing thickness.

The porosity and pore size distribution findings are shown in Figs. 4 and 5. Total sample porosities in the 1–100 nm pore diameter range followed much the same pattern as surface porosity in this range, rising with leaching time up to 9, 21 and 42 days in C_3S, WOPC and OPC, respectively, and subsequently declining (see Fig. 4). The pore size distribution curves in Fig. 5 show: (i) the disappearance of the population of 10–20 nm pores in the first 9 days of exposure, and a one order of magnitude rise in the number of pores with a diameter of 3–5 nm; (ii) in C_3S, a progressive shift in this kind of pores to values of 10–20 nm after 21 days and 20–30 nm after 42 and 63 days of exposure to leaching; (iii) in OPC, relative stability in the quantity of small pores up to 42 days of leaching, with only a minor enlargement, to 8 nm; (iv) a similar pattern in WOPC, although with a shift to higher values (10–20 nm).

Two hypotheses might be exposed to explain the changes induced in the pore structure by leaching. According to the first hypothesis, during short periods of exposure, the population of larger (10–20 nm) pores, associated with a more porous or less dense gel (LP–C–S–H gel) is transformed into a denser, LD–C–S–H type structure. This LD structure is vulnerable, however, and decays as leaching progresses, particularly in the C_3S paste. This hypothesis is consistent with an increase in gel polymerisation prompted by the decline in its Ca/Si ratio, as verified by BSEM analyses, and a change in the 5-nm gel droplets into laminates. The second hypothesis would be consistent with the results reported by Thomas et al. [33]: the 10–20 nm diameter pores disappear early because they are more vulnerable to attack and convert into larger pores (no capillary pores were detected by BET). The population of smaller pores (with a diameter of 3–5 nm), associated with the outer product, low density product (LD–C–S–H gel), grows by one order of magnitude as a result of the transformation of HD–C–S–H into LD–C–S–H gel. According to Chen et al. [19], the destruction of the LD structure after longer exposure to leaching, observed in the C_3S only, may be associated with the loss of Ca in the gel interstices, narrowing the inter-laminar space and causing shrinkage.

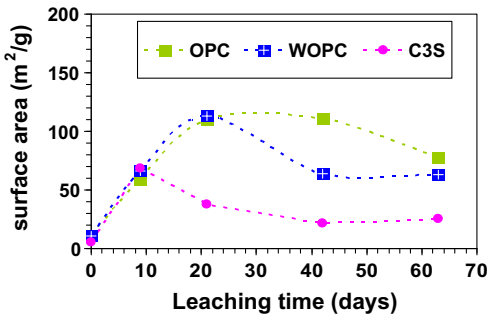

Fig. 3. OPC, WOPC and C_3S surface area versus leaching time.

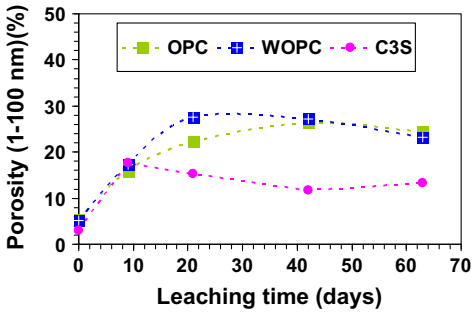

Fig. 4. OPC, WOPC and C_3S nanoporosity versus leaching time.

On the grounds of the changes observed in the three materials studied, they can be ranked by descending order of leach resistance as follows: OPC > WOPC > C_3S.

3.4. X-ray diffraction and FTIR analysis

The XRD patterns and FTIR spectra for C_3S, OPC and WOPC pastes before and after exposure to the ammonium nitrate leaching solution are shown in Fig. 6. The XRD patterns for all the pastes exposed to the aggressive solution revealed the existence of substantial amounts of amorphous phase. An amorphous halo appeared after 9 days of interaction with the aggressive solution, normally at $2\theta = 25–35°$, and grew with time.

In addition to the amorphous halo, a series of reflections were detected on the 9-day C_3S diffractograms (see Fig. 6a) that denoted the presence of crystalline compounds forming during the 6-M NH_4NO_3 attack. The portlandite observed in the pattern for the control C_3S (t0) was not detected, although traces of C_3S were found, indicating that dissolution progressed in the unhydrated phases as well. Calcite, a result of sample carbonation, was identified, along with two calcium silicate hydrates: CSH_1, $CaO.SiO_2.H_2O$, and CSH_2 or Riversideite, $2CaSiO_3{\cdot}3H_2O$, both of whose Ca/Si ratios were approximately 1. The 21-day diffractogram exhibited a similar pattern. This paste became more amorphous after 42 and 63 days, when reflections were observed for only one gel (CSH_1). The FTIR findings for the same pastes confirmed the XRD results. The band attributed to portlandite (3643 cm^{-1}) disappeared after 9 days. The band at around 970 cm^{-1} characteristic of the asymmetric stretching vibrations (υ_3 Si–O) in the C–S–H gel shifted with time to a higher wave number (963 cm^{-1} at time 0 to 973 cm^{-1} after 63 days). In contrast, the band at 455 cm^{-1}, attributed to υ_4 Si–O–Si (SiO_4) bending vibrations, grew more intense and shifted to 463 cm^{-1}, indicating a change in the C–S–H gel due to decalcification and the formation of a silica gel. The wide band at around 1074–1081 cm^{-1} had a shoulder at 1210 cm^{-1} attributable to a gel-like substance (υ_3 Si-O). The interaction with the leaching solution led to the presence of a very prominent band assigned to calcium nitrates: a wide band centred at 1384 cm^{-1}, characteristic of the asymmetric stretching vibrations (υ_3) in the (NO_3^-) groups present in hydrated $Ca(NO_3)_2$. These nitrates were not detected on the XRD patterns.

Significant changes were observed with time in the XRD patterns for the OPC pastes in contact with the aggressive NH_4NO_3 solution (Fig. 6b). As with the C_3S, the 9-day diffractogram revealed that the sample had grown more amorphous due to decalcification, with the near disappearance of the diffraction lines associated with portlandite, $Ca(OH)_2$. The amorphous halo was observed to grow, probably due to the formation of a silica gel type-phase, while the reflections for ettringite ($3CaO{\cdot}Al_2O_3{\cdot}3CaSO_4{\cdot}32\ H_2O$) were more intense after 9 and 21 days of leaching. The diffraction line for an aluminium-rich compound, aluminium oxide (JCPDS 10-0414),

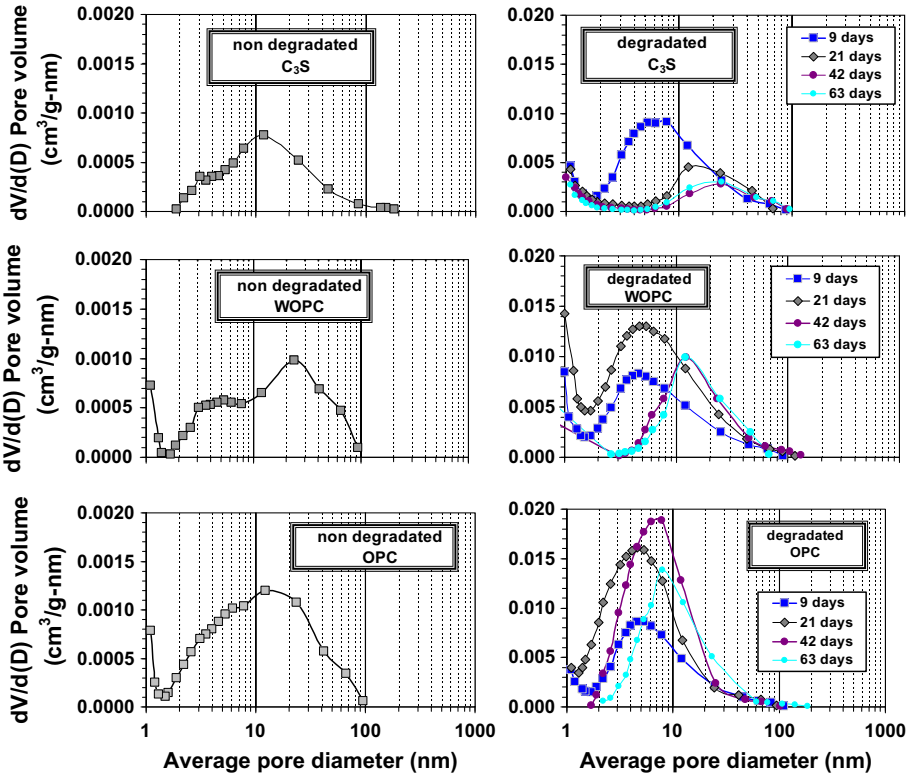

Fig. 5. Pore size distribution curves for non-decayed and decayed C_3S, OPC and WOPC pastes.

was likewise more intense after 9 days of exposure to the ammonium nitrate. After 21 days of interaction with the aggressive medium, low intensity reflections were still detected for anhydrous silicate and alite, while substantial amounts of amorphous phase were observed to form. The decalcification of C–S–H gel entailed the formation of HSi or hydrogen silicate hydrate gel (JCPDS 35-0062) whose formula is $H_4Si_8O_{18}{\cdot}H_2O$. Ettringite was no longer present in the 42-day patterns. As noted earlier, this may have been due to the change in the NH_4NO_3 solution pH to over 9.2, observed 30 days into the test, which necessitated replacement with a fresh solution. The change in pH, in conjunction with the decline in the concentration of the dissolved ions, may have prompted ettringite decomposition [30]. Portlandite and C–S–H gel dissolution upon interaction with the aggressive NH_4NO_3 solution logically induced the formation of hydrated calcium nitrates. While readily detected with FTIR, these compounds were not present in high enough concentrations for their crystalline form to be detected with XRD. As the cement-aggressive medium interaction progressed, the band at around 970 cm^{-1} characteristic of C–S–H gel asymmetric stretching vibrations (υ_3 Si–O) shifted to higher wave numbers (977 cm^{-1} at time 0–986 cm^{-1} at 9 days, 1008 cm^{-1} at 21 days and 1012 cm^{-1} at 42 and 63 days). This would appear to indicate that the gels formed after 63 days were the same as after 42 days and that aggressive medium-induced decalcification proceeded in these hydration products. The ongoing attack gave rise to a silica gel, detected on the 42- and 63-day spectra as vibrations at 1012 cm^{-1}. This also denoted decalcification of the C–S–H gel after 42 days of exposure to the aggressive medium and the formation, over time, of the silica gel (intensification of the SiO_4 band). Calcium nitrate and ammonium sulphate formation, not observed in the XRD findings, was also detected in the FTIR spectra for the OPC pastes in the form of a wide band centred at 1385 cm^{-1}, characteristic of the asymmetric stretching vibrations (υ_3) in the (NO_3^-) groups in $Ca(NO_3)_2$. According to the XRD findings, ettringite disappeared after 42 days, and no band at 1113 cm^{-1} was observed on the spectra. However, a shoulder detected at 1165 cm^{-1} was attributed to the S–O asymmetric stretching vibrations (υ_3) in $(NH_4)_2SO_4$. The presence of this phase was also confirmed by the shoulder at around 1400 cm^{-1} attributed to (N–H)υ_4 vibrations in the NH_4 in $(NH4)_2SO_4$ and the wide band at 3220 cm^{-1} attributed to the (N–H)υ_3 vibrations characteristic of the NH_4 in this compound [31,32].

Fig. 6c compares the XRD patterns for WOPC pastes before and after interaction with the aggressive ammonium nitrate solution. Decalcification took place via a reaction similar to the reaction described above for OPC. The FTIR spectra for these samples showed that the band at around 970 cm^{-1} characteristic of the asymmetric stretching vibrations (υ_3 Si–O) in C–S–H gel exhibited a larger shift with exposure time to the cement-aggressive medium than the analogous band in the OPC spectra, and reached higher wave numbers (975 cm^{-1} at 9 days, 1036 cm^{-1} at 21 days and 1047 cm^{-1} at 42 and 63 days). This provided further evidence of C–S–H gel decalcification and the formation of a silica gel, as detected with XRD techniques. $Ca(NO_3)_2$ and $(NH_4)_2SO_4$ were also detected on these spectra.

Pursuant to these mineralogical results, the reaction between the ammonium nitrate solutions and the main hydrated cement phases (CH, C–S–H gel and ettringite) are deduced to have taken place as follows:

$$Ca(OH)_2 + 2NH_4NO_3 \rightarrow Ca(NO_3)_2 + 2NH_3 + 2H_2O \quad (2)$$

$$xCaO \cdot SiO_2 \cdot xH_2O + NH_4NO_3 \rightarrow SiO_2 \cdot yH_2O + Ca(NO_3)_2 + NH_3 + H_2O \quad (3)$$

$$3CaO \cdot Al_2O_3 \cdot 3CaSO_4 \cdot 32H_2O + NH_4NO_3 \rightarrow (NH_4)_2SO_4 + Ca(NO_3)_2 + Al_2O_3 \cdot xH_2O + (32 - x)H_2O \quad (4)$$

The dissolution of portlandite and the decalcification of C–S–H gel in cement pastes have been described by other authors [22–26]. Fewer studies have addressed the effect of Ca leaching

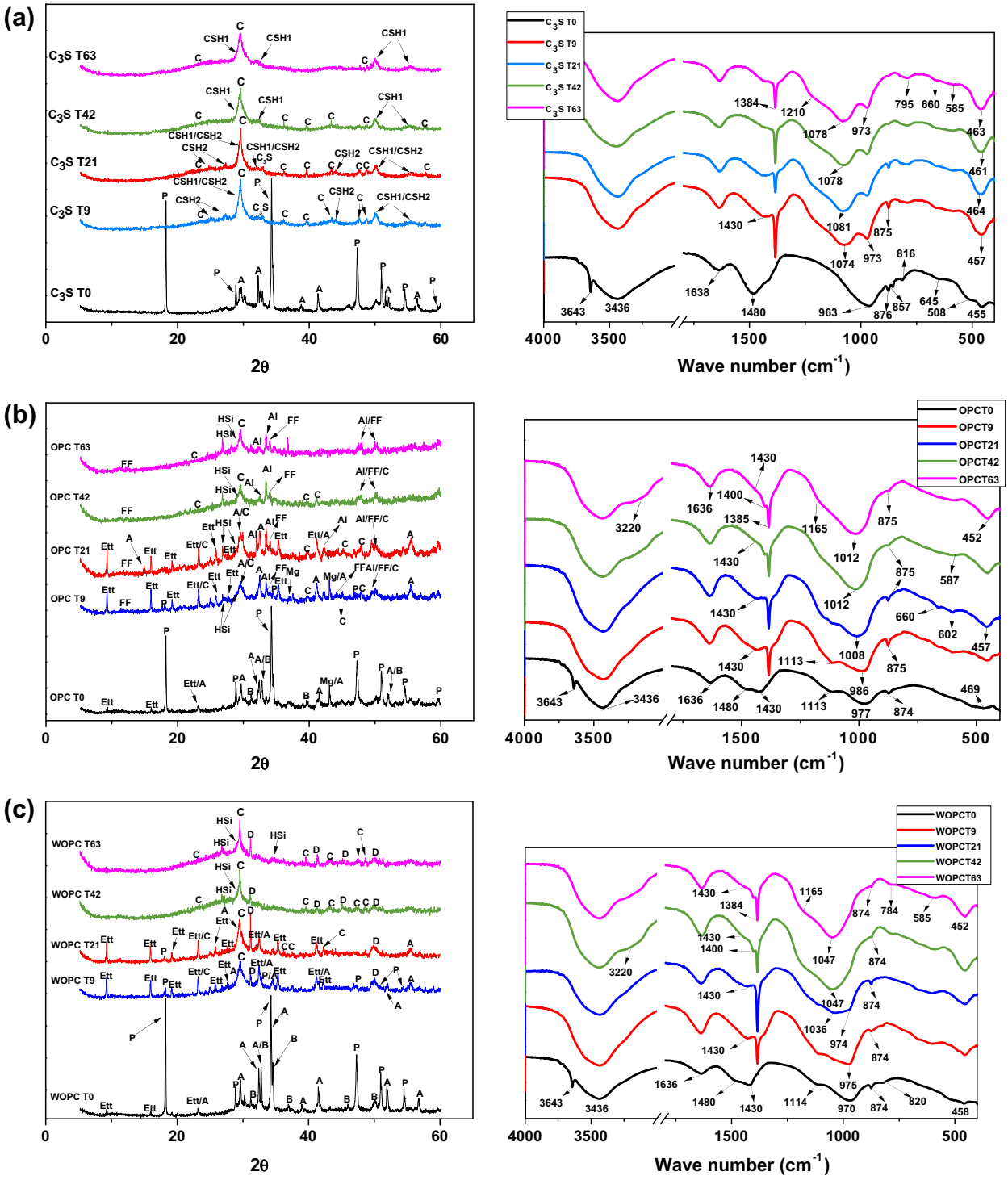

Fig. 6. XRD patterns and FTIR spectra for: (a) C_3S, (b) OPC and (c) WOPC specimens hydrated for 28 days: control and after interaction with the aggressive medium for 9, 21, 42 and 63 days. A: Alite, B: Belite; C_3S; C: Calcite; P: Portlandite; CSH1: Calcium silicate Hydrate, CSH2: Riversideite.

on ettringite phases. The present findings showed OPC pastes to be more leach-resistant than WOPC pastes, and the C_3S pastes to be the least resistant of the three materials.

3.5. BSEM/EDX analysis

The samples exposed to the NH_4NO_3 solution for 9 days were analysed with BSEM/EDX after impregnation in epoxy resin, polishing and carbon coating. The pink stain in the OPC sample shown in Fig. 7 defines the core or unaltered area, while the lighter colour in the rest of the specimen denotes alteration. The BSEM images in the figure reveal the morphological change induced by the aggressive agent deep within the sample. Porosity increased and both the anhydrous and hydrated phases dissolved.

As expected, the Ca/Si ratios of the pastes rose on an inward gradient, from the surface to the unaltered core of the specimen. This study was conducted on all three pastes. The most prominent difference was that after 9 days, the C_3S samples had been altered

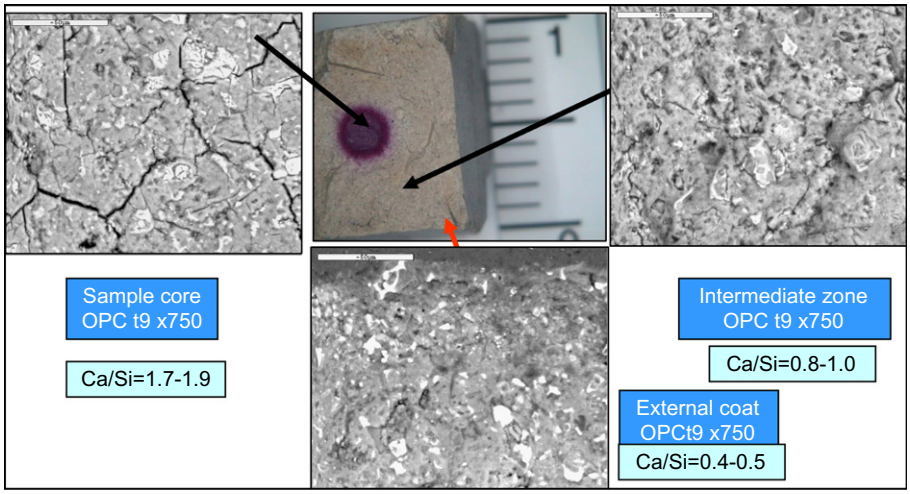

Fig. 7. BSEM images of OPC specimens after 9 days of exposure to 6-M NH_4NO_3. EDX analysis.

Table 3
Ca/Si ratio for C_3S, OPC and WOPC pastes after 9 days of exposure to 6 M-NH_4NO_3 solutions.

mm	C_3S	OPC	WOPC
5.0 (Sample core)	0.5–0.6	1.7–1.9	1.5–1.6
4.0	0.5–0.6	1.3–1.5	1.1–1.3
3.0 (Intermediate zone)	0.5–0.6	0.8–1.0	0.7–0.9
1.5	0.3–0.4	0.5–0.7	0.5–0.6
0.5 (Outer coating)	0.1–0.2	0.4–0.5	0.1–0.2

through to the core. The depth gradients for the Ca/Si ratios in the C_3S, OPC and WOPC pastes are given in Table 3. These findings confirmed that C–S–H gel decalcification was more intense in the WOPC than in the OPC pastes, very likely due to the higher Ca content in white cement. More severe decalcification was observed in the C_3S paste, whose Ca content and solubility are higher than in either of the cements. These specimens (C_3S pastes) were nearly completely decalcified after 9 days and exhibited Ca/Si ratios across the entire specimen between 0.5 and 0.1.

4. Conclusions

The main conclusions drawn from the present study are:

(i) Calcium leaching-induced decay in the cementitious materials studied (C_3S, OPC and WOPC), accelerated by immersion in ammonium nitrate, affected the main calcium phases in the samples (CH, C–S–H gel and ettringite), i.e., the anhydrous and hydrated phases.

(ii) After 21 days of Ca leaching, portlandite and ettringite disappeared from the OPC and WOPC pastes, and silica gels and low Ca/Si ratio C–S–H gels formed. Ca leaching is a coupled diffusion–dissolution process exhibiting interaction fronts that advance evenly across the material. The present study showed that the Ca/Si ratio of the gels declined on a gradient from the sample core outward.

(iii) The ammonium nitrate solutions reacted with the main hydrated cement phases (CH, C–S–H gel and ettringite) as follows:

$$Ca(OH)_2 + 2NH_4NO_3 \rightarrow Ca(NO_3)_2 + 2NH_3 + 2H_2O$$

$$xCaO \cdot SiO_2 \cdot xH_2O + NH_4NO_3 \rightarrow SiO_2 \cdot yH_2O + Ca(NO_3)_2 + NH_3 + H_2O$$

$$3CaO \cdot Al_2O_3 \cdot 3CaSO_4 \cdot 32H_2O + NH_4NO_3 \rightarrow (NH_4)_2SO_4 + Ca(NO_3)_2 + Al_2O_3 \cdot xH_2O + (32 - x)H_2O$$

(iv) After leaching, the population of 10–20 nm pores disappeared, while an increase by one order of magnitude was observed in pores with a diameter of 3–5 nm. Specimen surface area and nanoporosity rose in cementitious materials after Ca leaching-induced decay and then declined as a result of the collapse of the hydrated cement structure, primarily the C–S–H gel.

(v) Leaching impacted C_3S paste more quickly and intensely than WOPC or OPC pastes. On the grounds of the present findings, leach resistance in these materials can be ranked as follows: OPC > WOPC > C_3S.

Acknowledgment

The present study received financial support from the EU under Contract NMP3-SL-2008-214030.

References

[1] Metha PK. Durability of concrete – fifty years of progress? In: Malhotra VM, editor. Durability of concrete, second international conference, Montreal Canada, vol. 1. ACI SP 126; 1991. p. 696.
[2] Glasser FP, Marchand J, Samson E. Durability of concrete-degradation phenomena involving detrimental chemical reactions. Cem Concr Res 2008;38:226–46.
[3] LEÁS. Chemistry of cement and concrete. In: Hewlett Meter C, editor. 4th ed.; 1988.
[4] Neville AM, Brooks JJ. Concrete technology. 2nd ed. Longman Group; 1987.
[5] Metha PK. Concrete: structure, properties and materials. New York: Prentice-Hall, mInc. Englewood Cliffs; 1986.
[6] Skalny J, Marchand J, Older I. Sulfate attack of concrete. London: E&FN Spon; 2001.
[7] Skalny J, Johansen V, Thaulow N, Palomo A. DEF: as a form of sulfate attack. Mater Constr 1996;46(244):5–29.
[8] Davis D, Oberholter RE. Alkali-silica reaction products and their development. Cem Concr Res 1988;18:621–35.
[9] Saito H, Nakane S, Ikari S, Fujiwara A. Preliminary experimental study on the deterioration of cementitious materials by an acceleration method. Nucl Eng Des 1992;138:151–5.
[10] Berner UR. Evolution of pore water chemistry during degradation of cement in a radioactive waste repository environment. Waste Manage 1992;12:201–19.
[11] Atkins M, Glasser FP, Kindness A. Cement hydrated phases: solubility at 25 °C. Cem Concr Res 1992;22:241–6.
[12] Chen JJ, Thomas JJ, Taylor HFW, Jennings HM. Solubility and structure of calcium silicate hydrate. Cem Concr Res 2004;34:1499–519.
[13] Perkins RP, Palmer CD. Solubility of ettringite ($Ca_6[Al(OH)_6]_2(SO_4)3\ 26H_2$=) at 5–75 °C. Geochim Cosmochim Acta 1999;63:1969–80.

[14] Maltais Y, Samson E, Marchand J. Predicting the durability of Portand cement systems in aggressive environments-laboratory validation. Cem Concr Res 2004;34:1579–89.
[15] Matschei T, Lothenbach B, Glasser FP. The AFm phase in Portland cement. Cem Concr Res 2007;37:118–30.
[16] Glasser FP, Marchand J, Samson E. Durability of concrete – degradation phenomena involving detrimental chemistry reactions. Cem Concr Res 2008;38:226–46.
[17] Goñi S, Hernández MS, Guerrero A, Lorenzo MP. Effect of temperature on the leaching performance of a simulated cement-based immobilization system. Calcium and hydroxyl behaviour. Constr Build Mater 1996;10:171–7.
[18] Garrabrants AC, Sánchez F, Kosson D. Leching model for a cement mortar exposed to intermittent wetting and drying. AIChE J 2003;49(5):1317–33.
[19] Chen JJ, Thomas JJ, Jennings HM. Decalcification shrinkage of cement paste. Cem Concr Res 2006;36:801–9.
[20] Palacios M, Puertas F. Effect of carbonation on alkali-activated slag paste. J Am Ceram Soc 2006;89(10):3211–21.
[21] Puertas F, Palacios M, Vázquez T. Carbonation process of alkali-activated slag mortars. J Mater Sci 2006;41(810):3071–82.
[22] Harris AW, Manning MC, Tearle WM, Tweed CJ. Testing of models of the dissolution of cements-leaching of synthetic CSH gels. Cem Concr Res 2002;32:731–46.
[23] Haga K, Sutou S, Hironaga M, Tanaka S, Nagasaki S. Effects of porosity on leaching of Ca from hardened ordinary Portland cement paste. Cem Concr Res 2005;35:1764–75.
[24] Carde C, François R, Torrenti JM. Leaching of both calcium hydroxide and C–S–H from cement paste: modelling the mechanical behaviour. Cem Concr Res 1996;28(8):1257–68.
[25] Carde C, François R. Effect of the leaching of calcium hydroxide from cement paste on mechanical and physical properties. Cem Concr Res 1997;27(4):539–50.
[26] Heukamp FH, Ulm FJ, Germain JT. Mechanical properties of calcium-leached cement pastes. Triaxial stress states and the influence of the pore pressures. Cem Concr Res 2001;31:767–74.
[27] Faucon F, Adenot F, Jacquinot JF, Virlet J, Cabrillac R, Jorda M. Contribution of nuclear magnetic resonance techniques to the study of cement paste water degradation. In: Proc of the 10th international congress, 3, Gothenborg, Sweden; 1997. p. 3v003.
[28] Adenot F. Modelling of the corrosion of the cement paste by deionized water. Cem Concr Res 1992;22:489–96.
[29] Goñi S, Puertas F, Hernández MS, Palacios M, Guerrero A, Dolado JS, et al. Quantitative study of hydration of C_3S and C_2S by thermal analysis. Evolution and composition of C–S–H gels formed. J Therm Anal Calorim 2010;102(3):965–73. doi:10.1007/s10973-010-0816-7.
[30] Myneni SCB, Traina SJ, Logan TJ. Ettringite solubility and geochemistry of the $Ca(OH)_2$-$Al_2(SO_4)_3$–H_2O system at 1 atm and 298K. Chem Geol 1998;148:1–19.
[31] Nakamoto K. Infrared spectra of inorganic and coordination compounds. New York, London: John Wiley & Sons, Inc.; 1963.
[32] Gadsden JA. Infrared spectra of minerals and related inorganic compounds. Butterworths; 1975.
[33] Thomas JJ, Chen JJ, Allen AJ, Jennings HM. Effects of decalcification on the microstructure and surface area of cement and tricalcium silicate pastes. Cem Concr Res 2004;34:2297–307.
[34] Constantinides G, Ulm F-J. The effect of two types of C–S–H on the elasticity of cement-based materials: results from nanoindentation and micromechanical modelling. Cem Concr Res 2004(34):67–80.
[35] Gaitero JJ, Campillo I, Guerrero A. Reduction of the calcium leaching rate of cement paste by addition of silica nanoparticles. Cem Concr Res 2008;38:1112–8.
[36] Barret EP, Joyner LG, Halenda PP. The determination of pore volume and area distributions in porous substances. J Amer Chem Soc 1951;73:373–81.
[37] Brunauer S, Emmett PH, Teller E. Adsorption of gases in multimolecular layers. J Amer Chem Soc 1938;60:309–19.
[38] Harkins WD, Jura G. Vapor adsorption method for the determination of the area of a solid without the assumption of a molecular area, and the areas occupied by nitrogen and other molecules on the surface of a solid. J Amer Chem Soc 1944;66:1366–73.